TU Delft

Delft University of Technology

Document Version
Final published version

Licence
Dutch Copyright Act (Article 25fa)

Citation (APA)
Schneider, A., Diehl, P., Reiter, J., Ferrer-Carbonell, C., Paul, C. E., & Hauer, B. (2026). Biocatalytic Access to Natural Mosquito Repellent p-Menthane-3,8-diol via Direct Asymmetric Prins Cyclohydration. *Angewandte Chemie - International Edition*, *65*(23), Article e8826784. https://doi.org/10.1002/anie.8826784

Important note
To cite this publication, please use the final published version (if applicable).
Please check the document version above.

Copyright
In case the licence states “Dutch Copyright Act (Article 25fa)”, this publication was made available Green Open Access via the TU Delft Institutional Repository pursuant to Dutch Copyright Act (Article 25fa, the Taverne amendment). This provision does not affect copyright ownership.
Unless copyright is transferred by contract or statute, it remains with the copyright holder.

Sharing and reuse
Other than for strictly personal use, it is not permitted to download, forward or distribute the text or part of it, without the consent of the author(s) and/or copyright holder(s), unless the work is under an open content license such as Creative Commons.

Takedown policy
Please contact us and provide details if you believe this document breaches copyrights.
We will remove access to the work immediately and investigate your claim.

This work is downloaded from Delft University of Technology.

Check for updates

Angewandte Chemie International Edition

Angewandte International Edition Chemie

How to cite: *Angew. Chem. Int. Ed.* **2026**, e8826784
doi.org/10.1002/anie.8826784

RESEARCH ARTICLE

Biocatalytic Access to Natural Mosquito Repellent *p*-Menthane-3,8-diol via Direct Asymmetric Prins Cyclohydration

Andreas Schneider[1,2] | Patricia Diehl[2] | Jessica Reiter[1] | Claudia Ferrer-Carbonell[3] | Caroline E. Paul[3] | Bernhard Hauer[1,2,4]

[1]Institute of Biochemistry and Technical Biochemistry, University of Stuttgart, Vaihingen, Germany | [2]Institut für Biotechnologie und Wirkstoff-Forschung gGmbH, Mainz, Germany | [3]Department of Biotechnology, Delft University of Technology, Delft, Van der Maasweg, Netherland | [4]Institute of Molecular Physiology, Johannes-Gutenberg-Universität, Mainz, Germany

Correspondence: Andreas Schneider (schneider@ibwf.de) | Caroline E. Paul (C.E.Paul@tudelft.nl) | Bernhard Hauer (hauer@ibwf.de)

Received: 3 December 2025 | **Revised:** 10 March 2026 | **Accepted:** 17 March 2026

Keywords: insect repellents | PMD | brønsted acid catalysis | terpene cyclases | prins cyclization

ABSTRACT

Vector-borne diseases pose a rising global health challenge, necessitating the development of safe and effective pest protection agents. Here, we report a highly selective biocatalytic direct Prins cyclohydration for the synthesis of (1*R*)-*cis*-*p*-menthane-3,8-diol (PMD), a natural insect repellent with high efficacy. By strategically engineering squalene-hopene cyclases (SHCs), we achieved >96% diastereomeric excess, surpassing previous synthetic methods. Structural and mechanistic analyses suggest direct Prins cyclohydration and a precisely positioned water molecule within the enzyme's active pocket adjacent to the final carbocation that drives hydration and catalytic efficiency. Fine-tuning the biocatalytic setup enabled preparative scale production, without losing much product selectivity. Moreover, we demonstrate access to the other naturally occurring PMD isomers from (*R*)- and (*S*)-citronellal, as well as a one-pot cascade starting from *E*/*Z*-citral. This study paves the way for highly selective access to stereodefined terpene-derived repellents and establishes engineered squalene-hopene cyclases as a tool for direct asymmetric Prins cyclohydration.

1 | Introduction

Vector-borne diseases like malaria, dengue, and Zika remain a pressing global health challenge, exacerbated by climate change expanding mosquito habitats [1, 2]. Repellents are the first line of defense, with *N*, *N*-diethyl-*m*-toluamide (DEET) (Figure 1A) reigning as the gold standard due to the low price and high efficiency [3, 4]. However, concerns over toxicity and environmental impact fuel the search for safer, sustainable alternatives [5, 6]. The sole approved natural repellent, *p*-menthanediol **1** (PMD, Figure 1A), is typically marketed as a stereoisomeric mixture and is widely used in consumer formulations (e.g., Anti-Brumm Naturel or MyggA Natural). Besides mosquitoes, repellency effects have been studied against a broad range of organisms, like ticks [7], bed bugs [8], biting midges [9], or head lice [10]. Notably, Borrego et al. demonstrated that the stereoisomer (1*R*)-*cis*-PMD **1** boosts the repellent efficiency by up to 50%, rivaling synthetic alternatives, like DEET [11, 12]. Access to stereodefined PMD is therefore valuable not only for synthesis, but also to enable analytical and performance benchmarking of individual stereoisomers across organisms and formulations. However, access to pure material is currently limited due to the absence of a selective synthesis method. PMD naturally arises via citronellal **2** aging in *Eucalyptus citriodora*, a process

© 2026 Wiley-VCH GmbH

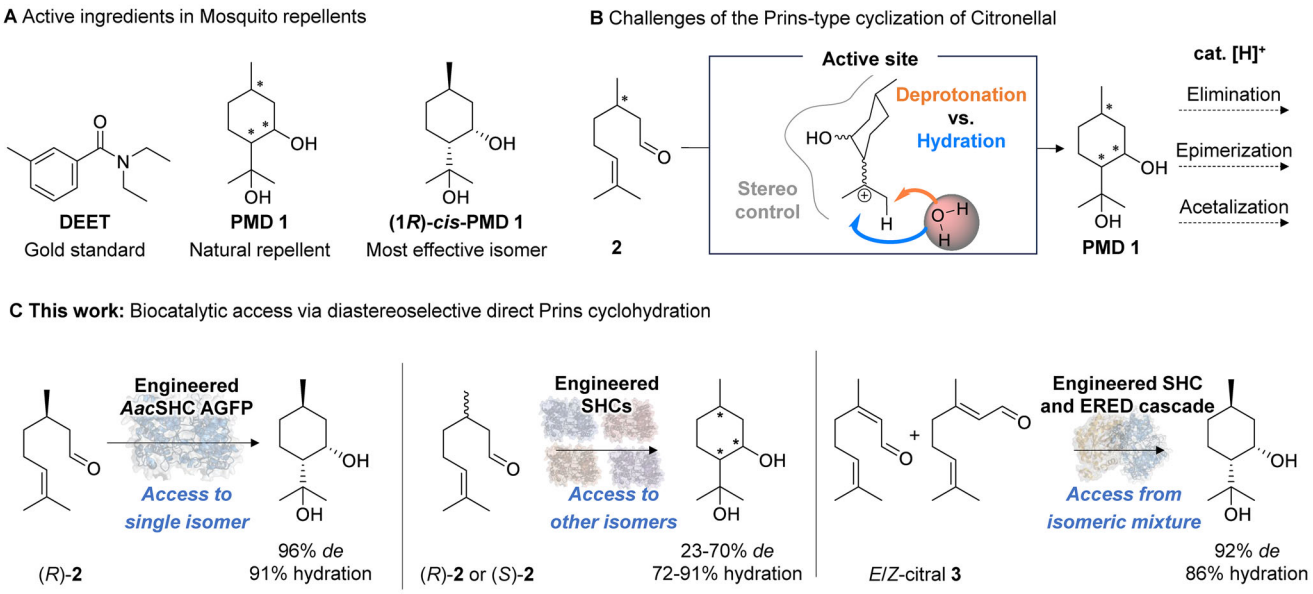


FIGURE 1 | Accessing Natural Mosquito Repellent (1*R*)-*cis*-*para*-menthane-3,8-diol (PMD) **1**. (A) Active ingredients in mosquito repellents: DEET and PMD 1 as well as the most effective enantiomer (1*R*)-*cis*-PMD **1**. (B) Challenges in the Brønsted acid catalyzed Prins cyclization of citronellal **2** arise as stereocontrol, regiocontrol (hydration vs. deprotonation), elimination, epimerization and acetalization. The carbocation quenching water molecule is shown as a red sphere. (C) This work: Biocatalytic access to natural mosquito repellent (1*R*)-*cis*-PMD **1** and other isomers via engineered squalene-hopene cyclases (SHCs). A one-pot two-enzyme ERED/SHC cascade starting from *E*/*Z*-citral 3 is also demonstrated.

accelerated by Brønsted or Lewis acid catalysis through a Prins-type cyclization (Figure 1B).

The Prins reaction has emerged as a key synthetic methodology in organic chemistry [13], with recent advances in asymmetric catalysis enabling precise control over reactive carbocationic terpene intermediates. Grimm and colleagues employed confined imidodiphosphorimidate (IDPi) catalysts to cyclize neral to (1*R*,6*S*)-*trans*-isopiperitenol with >90% diastereomeric excess (*de*), demonstrating both stereochemical control and suppression of unwanted elimination reactions [14]. In their study on the Prins-cyclization of citronellal **2**, Hart-Cooper et al. achieved 76% *de* using a supramolecular capsule [15]. Contrary to expectations, studies revealed that the metallocage does not promote 3D preorganization of the substrate toward cyclization-prone conformations, highlighting the complexity of rational catalyst design for this intricate transformation [16]. As a result, while controlling the spatial arrangement of the terpene skeleton has been achieved, the direct asymmetric Prins cyclohydration remains challenging. Indeed, direct asymmetric Prins cyclohydration poses a general catalytic challenge: a reactive carbocation must be steered toward cyclization while selectively admitting and positioning water to outcompete deprotonation and elimination.

So far, among multiple cyclohydration strategies [17–21] (see Table S1), Borrego et al. reported the highest diastereoselectivity (76% *de*) through kinetic control using excess sulfuric acid at −78°C [11]. This study highlighted that besides regio- and stereoselectivity, the prevention of side reactions, including acetalization, epimerization, and dehydration under acidic conditions, complicates the catalysis (Figure 1B).

Nature provides an elegant blueprint for the selective quenching of carbocations with water through terpene cyclases. Building upon our previous work utilizing squalene-hopene cyclases (SHCs) as Brønsted acid biocatalysts for various cationic rearrangements [22, 23], including Prins cyclizations [24], we now report a biocatalytic direct Prins cyclohydration yielding (1*R*)-*cis*-PMD **1** with 96% *de* and 91% hydration (Figure 1C). This study further elucidates how enzyme engineering enabled the development of a catalyst with excellent regio- and diastereoselectivity, addresses challenges associated with scale-up, presents selective starting points for (*S*)-citronellal **2** cyclization, and provides a strategy for replacing (*R*)-citronellal **2** via a two-enzyme cascade starting from *E*/*Z*-citral **3**.

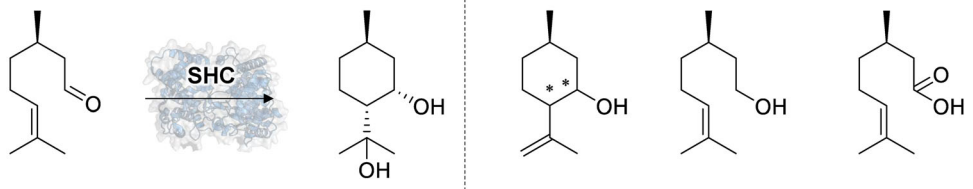
2 | Results and Discussion

2.1 | Establishing Reaction Conditions for Biocatalytic Cyclohydration of (*R*)-Citronellal 2

We began our study with a systematic evaluation of the biocatalytic reaction conditions in terms of GC conversion (GCC), hydration, and diastereomeric excess (*de*). Previously, we reported the Prins cyclization of (*R*)- and (*S*)-**2** using isolated *Aac*SHC (2-5 mol%) [24]. Under the described conditions (30°C), wild-type *Aac*SHC cyclized (*R*)-**2** exclusively to isopulegols **4**, thus favoring the deprotonation pathway (Table 1, Entry 1). Raising the temperature to 50°C shifted the reaction toward cyclohydration (53% hydration, 63% *de*, Entry 2). However, we noticed that the detergent-containing buffer alone drove most of the reaction (65% hydration, 71% *de*), highlighting the need for a more controlled approach (cf. Entries 3 and 4). The pronounced temperature dependence is consistent with a competition between (i) enzyme-guided cyclization and (ii) background Brønsted/Lewis-acid chemistry promoted by the micellar CHAPS system [25], motivating our shift to a whole-cell catalytic system.

15213773, 0, Downloaded from https://onlinelibrary.wiley.com/doi/10.1002/anie.882678 4 by Tu Delft, Wiley Online Library on [20/04/2026]. See the Terms and Conditions (https://onlinelibrary.wiley.com/terms-and-conditions) on Wiley Online Library for rules of use; OA articles are governed by the applicable Creative Commons License

TABLE 1 | Establishing reaction conditions for the biocatalytic cyclization of (*R*)-citronellal **2** with isolated *Aac*SHC or *E. coli* whole cells. Conditions: Entries 1 and 2: 1 mM (*R*)-**2**, 1% DMSO, 0.05 mM *Aac*SHC, 20 mM citrate, pH = 6.0, 0.2% CHAPS, 20 h, 200–250 rpm. Entries 4–13: 5 mM (*R*)-**2**, 1% DMSO, 50 mg_{CWW}/mL (or lyo: 10 mg_{CDW}/mL) *E. coli* whole cells expressing *Aac*SHC (0.05 mM), 100 mM citrate (or water), pH = 6.0, 72 h, 200 rpm. Given values represent the mean values of technical triplicates. KF = 100 mM potassium fluoride; γCD = 10 mM γ-cyclodextrin.



(*R*)-**2** (1*R*)-*cis*-**1** **4** **5** **6**

Entry	Conditions	GCC [%]	Hydration [%]	*de* [%]	Reduction [%]
1	*Aac*SHC, 30°C	1	—	33	—
2	*Aac*SHC, 50°C	24	53	63	—
3	CHAPS buffer[a], 50°C	23	65	71	—
4	*E. coli* buffer[b], 50°C	—	—	—	—
5	*E. coli*-*Aac*SHC, 30°C	—	—	—	>99
6	*E. coli*-*Aac*SHC, 50°C	—	—	—	>99
7	*E. coli*-*Aac*SHC-lyo[c], 30°C	17	34	83	27
8	*E. coli*-*Aac*SHC-lyo, water, 30°C	9	31	78	13
9	*E. coli*-*Aac*SHC-lyo, water, 50°C	12	29	75	7
10	*E. coli*-*Aac*SHC-lyo, KF, 50°C	15	27	74	<1
11	*E. coli*-*Aac*SHC-lyo, KF, γCD, 50°C	30	28	75	<1
12	*E. coli*-lyo, KF, γCD, 50°C	60	69	57	<1
13	*E. coli*-lyo, KF, γCD, 30°C	24	47	60	<1

[a]20 mM citrate, pH = 6.0, 0.2% CHAPS.
[b]100 mM citrate, pH = 6.0.
[c]10 mg_{CDW}/mL instead of 50 mg_{CWW}/mL; KF = 100 mM KF, γCD = 10 mM γ-cyclodextrin.

Knowing that SHCs exhibit distinct catalytic behavior in the presence of a biological membrane [26], we next explored whole-cell biocatalysis at 30°C using 50 mg_{CWW}/mL cells. However, a competing alcohol dehydrogenase (ADH) led to full reduction of (*R*)-**2** to (*R*)-citronellol **5**, which is a known challenge in the whole cell biotransformation of **2** [27]. Suppressing this side reaction required freezing (−20°C) or lyophilization overnight, and switching from citrate buffer to water, reducing unwanted reduction to 20% (freezing) and 13% (lyophilization), respectively (Entries 5 to 8, also see Table S2). Interestingly, adjusting the pH to 7.0 with TRIS or phosphate buffer reactivated redox activity, yielding both (*R*)-**5** and (*R*)-citronellic acid **6** as the main products. Carrying out the reaction at 50°C halved the reduction while only slightly increasing SHC activity (9% → 12% GCC, Entries 8 and 9). Since ADHs are known to be susceptible to salts [28], we screened a variety of salt additives. This approach revealed that fluoride salts (NaF or KF, 100 mM) minimize the background reduction, with KF even enhancing SHC activity (12% → 15% GCC, Entry 10, also see Tables S3 and S4).

To pinpoint the enzyme responsible for the reduction, we screened dehydrogenases of the *E. coli* Keio collection [29] and identified the malate dehydrogenase MaeB as the primary driver of reduction under our conditions (see Figure S1). However, comparing the introduced knockout strain *E. coli* BL21(DE3) ΔMaeB with *E. coli* BL21(DE3) did not show any changes in the background reduction behavior of the strain, which is most likely due to the different *E. coli* strains (K12 vs. BL21(DE3), see Table S5). Thus, we opted to proceed with the fluoride-based strategy.

Going forward, another challenge emerged during the biotransformation: acetalization of **1** with the substrate **2**, commonly reported in this transformation [11]. To mitigate this issue, we considered that encapsulation of the substrate/product could potentially reduce their inherent reactivity. Thus, we screened cyclodextrins (α, β, 2-hydroxypropyl-β, γ) and found that two equivalents of γ-cyclodextrin effectively suppressed dimerization from >35% to <1% while doubling conversion (15% → 30% GCC, Entry 11, see also Table S6). This optimization established our starting point: 30% GC conversion, 27% hydration, and 75% *de*. It should be noted that the lyophilized *E. coli* lacking heterologous expression of *Aac*SHC also facilitated cyclohydration with 57% *de* and 60% *de* at 50 and 30°C, respectively (Entries 12 and 13). We attribute this to a combination of background Brønsted/Lewis-acid catalysis and microenvironment effects in the lyophilized whole-cell matrix (e.g., local pH drift, metal ions, membrane/emulsification-assisted mass transfer, and endogenous components that can stabilize or quench carbocationic intermediates). Importantly, under the optimized conditions and with high SHC expression, the product distribution and

15213773, 0, Downloaded from https://onlinelibrary.wiley.com/doi/10.1002/anie.88267B4 by Tu Delft, Wiley Online Library on [20/04/2026]. See the Terms and Conditions (https://onlinelibrary.wiley.com/terms-and-conditions) on Wiley Online Library for rules of use; OA articles are governed by the applicable Creative Commons License

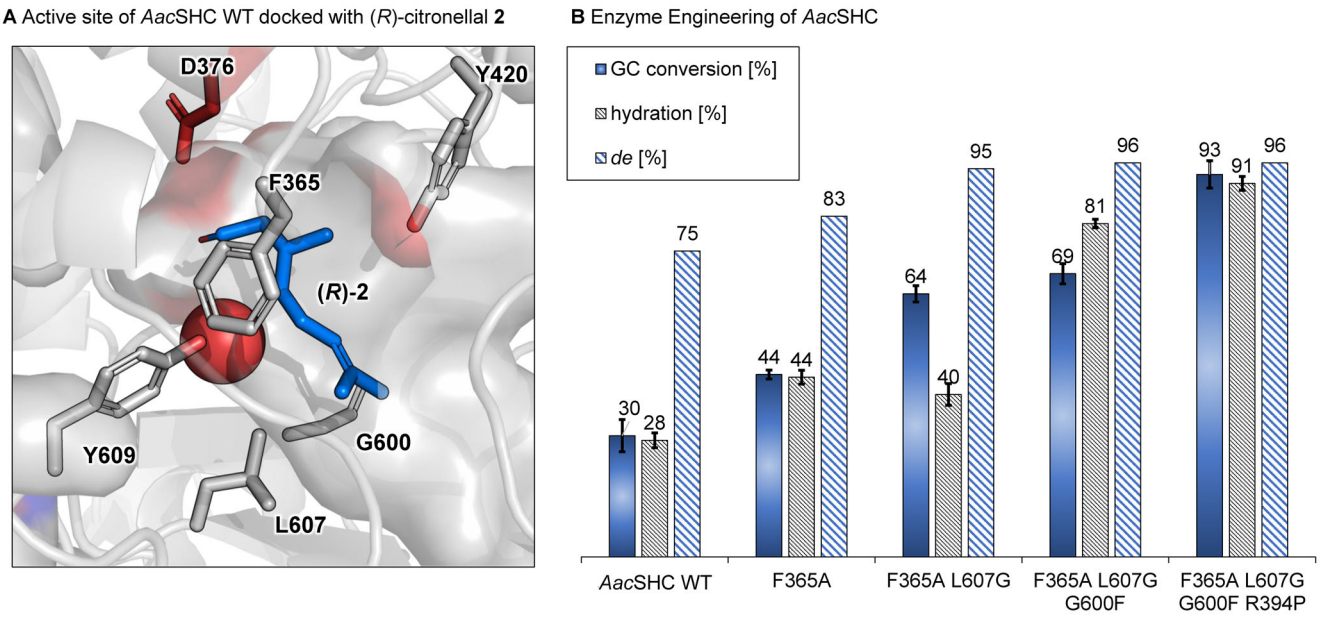


FIGURE 2 | Enzyme engineering of *Aac*SHC toward diastereoselective cyclohydration of (*R*)-**2**. (A) Active site of *Aac*SHC wild type (PDB: 1UMP) docked with (*R*)-**2** (blue sticks). Docking was performed with YASARA [30]. Highlighted are the protonating aspartate D376 (red sticks), as well as the discussed and engineered positions F365, Y420, G600, L607, and Y609. (B) Enzyme engineering scheme showing the improvements made for every variant in terms of GC conversion (n = 3, blue bars), hydration (n = 3, black striped bars), and diastereomeric access (blue striped bars). Reaction conditions: 10 mg_{CDW}/mL (0.01-0.05 mM *Aac*SHC), cells, 5 mM (*R*)-citronellal **2**, 1% DMSO, 100 mM KF, 10 mM γ-cyclodextrin, 50°C, 72 h. Unless stated otherwise, reported values represent the mean of technical replicates (n as indicated) and error bars denote the standard deviation.

stereoselectivity are dominated by the engineered enzyme, as reflected by the characteristic regio-/diastereoselectivity profile relative to the empty-vector control (see Figure 2). Finally, we validated the robustness of the reaction setup with a 96-deep well plate reaction, which resulted in a variation coefficient of 6% over the whole plate (see Figure S2).

2.2 | Enzyme Engineering Campaign toward Selective Formation of (1*R*)-*cis*-PMD 1

Using our established experimental setup, we evaluated the cyclization activity of various squalene-hopene cyclase (SHC) wild-type enzymes (see Table S7) and the previously identified *Aac*SHC variant F365A Y420W G600F (Figure 2A), which had demonstrated superior *cis*-selectivity in the cyclization of (*R*)-**2** [24]. All wild-type enzymes exhibited moderate to high diastereoselectivities (50%–84% *de*) and moderate regioselectivities (40%–75%) (see Table S7). When tested in the *E. coli* whole cell environment, the triple variant F365A Y420W G600F surprisingly showed 46% hydration with high diastereocontrol (81% *de*). Deconvolution of this triple variant revealed that the F365A mutation (83% *de*) was the primary contributor to diastereocontrol, while G600F had the most significant impact on enzyme regioselectivity, increasing from 28% hydration to 53%.

Subsequently, we performed rational saturation mutagenesis at position F365 to identify additional candidates for site-saturation mutagenesis. Most mutations at this position reduced all three parameters (GC conversion, regioselectivity, and diastereomeric excess). Solely F365Y performed comparably to F365A with 85% *de* and 42% hydration, though with approximately half the conversion of 21%. These results confirmed that F365A represented the optimal starting point, with 44% GC conversion, 44% hydration, and 83% *de* (Figure 2B).

We then performed transfer mutagenesis of the *Aac*SHC F365A mutation into the most promising wild-type enzymes (*Zmo*SHC1, *Zmo*SHC2, *Tel*SHC, *Sco*SHC) identified during screening, as this strategy led to superior enzymes in an earlier engineering campaign [23]. However, the F365A variant still emerged as the superior starting point for further engineering (see Table S7).

Next, we conducted site-saturation mutagenesis at positions G600 and L607, which were selected based on their proximity to the modeled substrate's prenyl moiety (Figure 2) and their successful targeting in previous engineering campaigns [22]. This strategy yielded variant F365A L607G with excellent diastereocontrol (95% *de*), 40% hydration, and 64% GC conversion. Combining this variant with G600F produced F365A L607G G600F, which more than doubled the hydration to 81% while improving both diastereoselectivity (96% *de*) and GC conversion (69%).

Subsequent site-saturation attempts at positions A306, F601, S307, and Y609 were unsuccessful. We therefore modified our approach by combining active site mutants with surface hot spot mutations predicted by FireProt. This software determines protein stabilizing mutations based on structural and evolutionary information [31, 32]. Five of nine resulting variants showed improved GC conversion, of which the R394P variant performed best in terms of GCC (see Table S8). Under the established conditions (Table 1, Entry 11), the surface mutation R394P enhanced GC conversion (93%) and hydration (91%) while maintaining a

15213773, 0, Downloaded from https://onlinelibrary.wiley.com/doi/10.1002/anie.8826784 by Tu Delft, Wiley Online Library on [20/04/2026]. See the Terms and Conditions (https://onlinelibrary.wiley.com/terms-and-conditions) on Wiley Online Library for rules of use; OA articles are governed by the applicable Creative Commons License

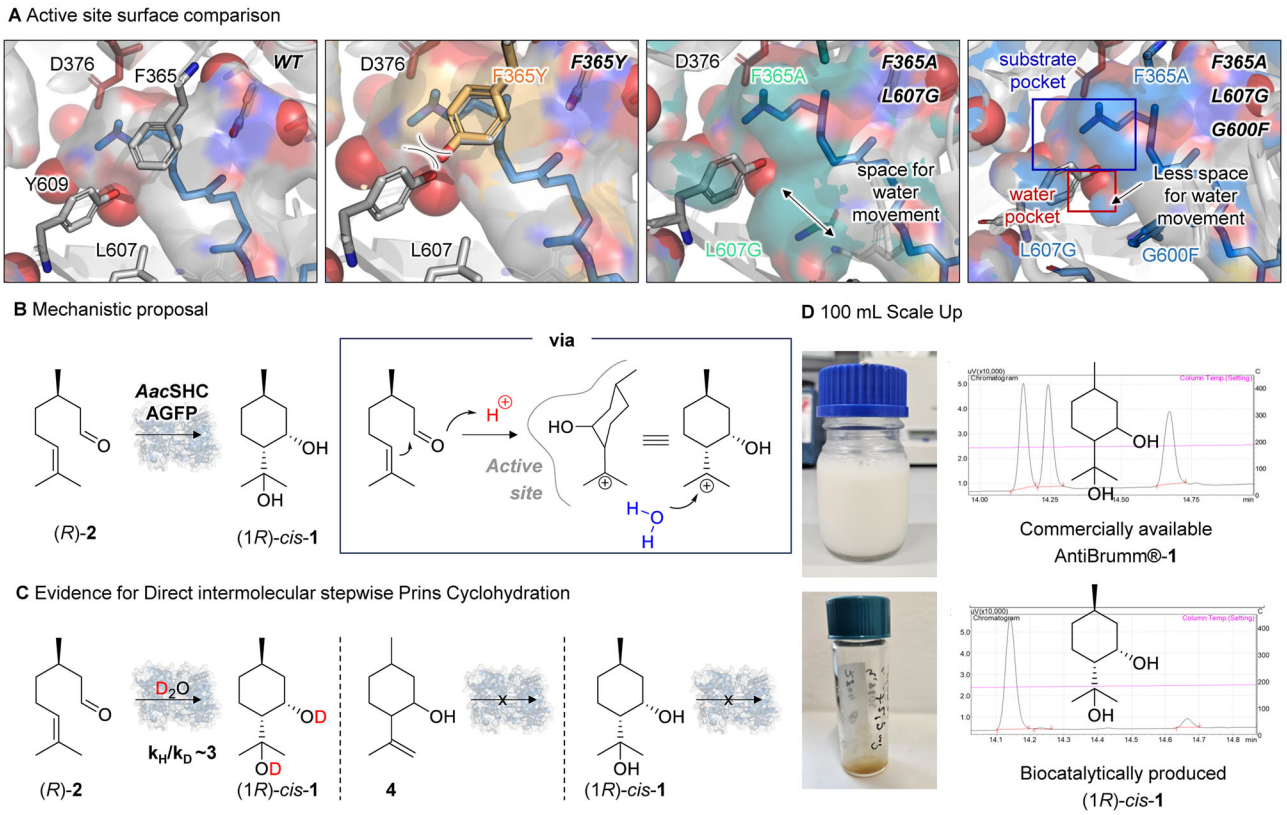


FIGURE 3 | Mechanistic investigation of direct Prins cyclohydration and upscaling of the reaction. (A) Active site surface overlay of *Aac*SHC wildtype (WT, grey) and variants F365Y (orange), F365A L607G (teal), and F365A L607G G600F (blue). The overlay demonstrates how the engineering potentially created a hydrophobic substrate pocket next to a precisely positioned water molecule. (B) Mechanistic proposal via Direct Prins cyclohydration. (C) The reaction in deuterium oxide (D_2O) with a kinetic isotope effect of $k_H/k_D \sim 3$ and the incorporation of two deuteriums emphasizes the intermolecular stepwise mechanism. Direct cyclohydration of (*R*)-**2** was further evidenced by incubation of isopulegol **4** with the *E. coli*-SHC setup, which showed no formation of (1*R*)-cis-PMD **1**. Epimerization and dehydration in the reaction setup were excluded by incubating product **1** in the *E. coli*-SHC setup. Conditions: 1 mM substrate, 1% DMSO, 10 mg_{CDW}/mL *E. coli* whole cells expressing *Aac*SHC AGFP, 100 mM KF, 10 mM γ-cyclodextrin, 40°C, 20 h, 250 rpm. For deuterium labeling and kinetic isotope effect determination, D_2O instead of H_2O was used. (D) Scale up of the biocatalytic reaction in a 100 mL Schott bottle. The extract was analyzed via chiral GC and compared with the commercially available mosquito spray Anti-Brumm Naturel. For detailed reaction setup, conditions, and extraction, see supplementary material.

de of 96% (Figure 2b). Isolation of variant F365A L607G G600F led to less selective enzyme behavior (91% *de*, 68% hydration, and 44% conversion, see Table S7), most likely due to the background reaction in the CHAPS buffer (see Table 1, Entry 3). No further improvements in catalytic parameters were achieved through additional engineering attempts, likely due to background activity from the *E. coli* cells. The engineering campaign was therefore concluded at this stage with the *Aac*SHC variant F365A L607G G600F R394P, that is, AGFP.

2.3 | Mechanistic Investigations on Enzymatic Direct Cyclohydration

To understand the structural basis for our observed catalytic improvements, we compared the active site architectures of the wild-type *Aac*SHC and variants F365Y, F365A L607G, and F365A L607G G600F, that is, AGF (Figure 3A). The wild-type active site is consistently depicted in grey, with variant structures overlaid and distinctively colored for visual differentiation. Co-crystallized water molecules are represented as red spheres. Structural analysis of the F365Y variant (orange surface) relative to wild-type revealed that the introduced hydroxyl group likely sterically repulses the hydroxyl group of Y609, creating an expanded pocket in this region, similar to that observed in the F365A variant (cf. Figure 3A, wild-type, F365Y, and AGF structures).

The L607G mutation further expands the pocket proximal to the water molecule adjacent to Y609, potentially facilitating water molecule mobility and allowing closer substrate positioning relative to this catalytic water. Both the F365A and L607G mutations appear to promote substrate orientation in the *cis* configuration, explaining the improved *de* of 95%.

The G600F mutation likely enables more precise positioning of the Y609-adjacent water molecule, accounting for the enhanced hydration efficiency (81%) and doubled regioselectivity. This water-positioning function of the G600F mutation was also apparent in the corresponding single variant (see Table S7). Based on these observations, we propose that the water molecule coordinated by Y609 serves as the nucleophile in the cyclization reaction. This hypothesis is further supported by the Y609F mutation, which shifted the reaction outcome toward 85% deprotonation (see Table S7). Further work to understand the precise

15213773, 0, Downloaded from https://onlinelibrary.wiley.com/doi/10.1002/anie.88267B4 by Tu Delft, Wiley Online Library on [20/04/2026]. See the Terms and Conditions (https://onlinelibrary.wiley.com/terms-and-conditions) on Wiley Online Library for rules of use; OA articles are governed by the applicable Creative Commons License

hydration vs. deprotonation dynamics within the SHC active site is currently ongoing.

The effect of the surface mutation R394P could not be directly rationalized through active site analysis, as it exerts no immediate influence on the active site cavity. The targeted 'RRRR' region is not situated at the oligomeric interface of *Aac*SHC and exhibits high sequence diversity among SHC congeners (see Figure S3). Nevertheless, the helix-disrupting proline substitution may enhance enzyme stability, consistent with previous findings from the Suzuki and Wu groups [33, 34].

Moving forward, we investigated the reaction mechanism by contrasting an intramolecular concerted carbonyl-ene cyclization with an intermolecular stepwise Prins-type cyclization (Figure 3B). First, we confirmed the intermolecular cyclohydration mechanism by conducting the reaction in D_2O, observing a +2 mass shift in the product mass spectrum (Figure 3C and Supplementary methods). In this course, we also determined a kinetic isotope effect of ~3, confirming the protonation to be rate-determining and providing evidence for a stepwise Prins-type reaction [35]. Knocking out the protonating aspartic acids D374A(X)D376AD377A of the SHC's protonation motif further rejects an intramolecular mechanism (see Table S7, "KO" enzyme). To verify that the reaction proceeds through direct cyclohydration rather than via isopulegol **4** intermediates, we incubated an isomeric isopulegol **4** mixture with our engineered variant, yielding no hydration product, which further supports the proposed mechanism (Figure 3C).

Known challenges in the cyclization of **2** toward **1** include acid-catalyzed epimerization and elimination reactions, both of which reduce product quality. Our enzymatic system successfully prevented these undesirable side reactions, as demonstrated by incubating product (1*R*)-*cis*-PMD-**1** with *E. coli*-*Aac*SHC AGFP (Figure 3C).

To assess scalability, we conducted reactions at 100 mL scales. Therefore, we first determined the favorable substrate concentration, having previously observed substrate inhibition in SHC-catalyzed in vivo reactions [36]. The results indicate optimal enzyme performance at ~5 mM substrate concentration (see Figure S4). Although the reaction gets faster with rising temperature (22°C to 60°C, TOF 0.2–1.5 h^{-1}), the product quality at 40°C was much better compared to 50°C (94% vs. 53% *de*), which is probably due to non-enzymatic background cyclization during the longer reaction time. (see Figure S4D). After 144 h, the reaction reached ~98% conversion (GC analysis) and was terminated by extraction with cyclohexane/ethyl acetate (1:1). The product was isolated in 80% yield (75.9 mg), 94% *de*, and 84% hydration. The long endpoint time in scale-up likely reflects a shift from intrinsic catalytic turnover to process limitations that become dominant at preparative volume, including substrate/product partitioning in a biphasic whole-cell system, membrane-associated mass transfer, progressive enzyme deactivation, and/or product inhibition as demonstrated in related studies from our group [22, 36].

Next, we evaluated our enzyme library to demonstrate the ability to produce the other PMD isomers via Direct Prins cyclohydration (Figure 4A). Interestingly, both *trans* isomers (1*R*)- as well as (1*S*)-*trans*-PMD were accessible via *Zmo*SHC1 mutants from earlier projects [37]: G667V (= G600V *Aac*SHC amino acid position, Figure 2A) for (1*R*)-*trans*-PMD (23% *de*), and G667L for (1*S*)-*trans*-PMD (70% *de*), respectively. The best candidate from our library to generate (1*S*)-*cis*-PMD was *Aac*SHC L36Q [38] with 53% *de*.

2.4 | Enzymatic One-pot Cascade From *E*/*Z*-citral

To improve the economic feasibility of (1*R*)-*cis*-PMD synthesis, we investigated the use of the ene reductase (ERED) Old Yellow Enzyme 2 (OYE2) from *Saccharomyces cerevisiae* with the variant Y83V [39], to stereoconvergently reduce the cheap and commercially available 60:40 *E*/*Z*-citral **3** to (*R*)-**2**. The starting material *E*/*Z*-citral **3** is industrially separated via distillation on a 100,000 t/a scale [40] before its hydrogenation to (***R***)- or (***S***)-**2**. Thus, the enzymatic one-pot cascade via stereoconvergent reduction followed by diastereoselective cyclohydration is appealing. In a time-course experiment, purified 0.1 mol% OYE2 Y83V converted 5 mM *E*/*Z*-**3%** to 95% (*R*)-**2** with 94% enantiomeric excess (*ee*) in 2.5 h using $NADP^+$ as cofactor (see Figure S5C). To check compatibility with our fluoride-based inhibition system of undesired endogenous enzymes, we screened various additives for their inhibitory effect on OYE2 Y83V (see Figure S5D). To our delight, 100 mM KF again turned out to be the most compatible with OYE2 Y83V, retaining its highest specific activity without losing its selectivity of 94% *ee*.

Having established the reaction conditions, we combined the *E. coli* whole cells expressing *Aac*SHC AFGP with OYE2 Y83V and glucose dehydrogenase (GDH) for NADPH recycling (Figure 4B). While no ene-reduction of **3** was observed at 50°C at any condition, adjusting the temperature to 40°C led to the desired (1*R*)-*cis*-PMD **1** albeit with 64% *de*, 72% hydration and 42% conversion under the best condition of 0.1 mol% OYE2 Y83V, 1 mM $NADP^+$, 1 U/mL GDH and 25 mM glucose (see Figure S18). Interestingly, doubling the GDH concentration led to a dramatic drop in overall performance, presumably due to increased background activity (see Figure S6). Moreover, halving the OYE2 concentration showed almost no difference in the cascade, thus highlighting the SHC as the bottleneck. As a result, we prepared spheroplasts from the *E. coli* whole cells (= *E. coli*$_{sp}$) to accelerate the *Aac*SHC, which proved as an efficient strategy in an earlier study [26]. This procedure led to an increase in *de* to 95% (Figure 4B, Condition A), while doubling the spheroplast concentration from 20 to 40 mg_{CWW}/mL yielded the best overall result of 92% *de*, 86% hydration, and 85% conversion within 96 h at 40°C (Condition B). Control reaction without the recycling system (Condition C) or OYE2 (Condition D) confirmed the necessity of all compounds in the cascade reaction. To our delight, the one-pot cascade only slightly falls behind the SHC solo reaction with 96% *de*, 91% hydration, and 93% conversion (cf. Figure 2, AGFP). Using *E. coli*$_{sp}$ not only improved the cascade but also made the overall system less prone to distortion from the other additives, that is, OYE2, GDH, or $NADP^+$ (see Figure S6 for more details).

3 | Conclusion

In this study, we have leveraged the precision of enzyme catalysis to overcome longstanding challenges in the selective Prins

15213773, 0, Downloaded from https://onlinelibrary.wiley.com/doi/10.1002/anie.202507804 by Tu Delft, Wiley Online Library on [20/04/2026]. See the Terms and Conditions (https://onlinelibrary.wiley.com/terms-and-conditions) on Wiley Online Library for rules of use; OA articles are governed by the applicable Creative Commons License

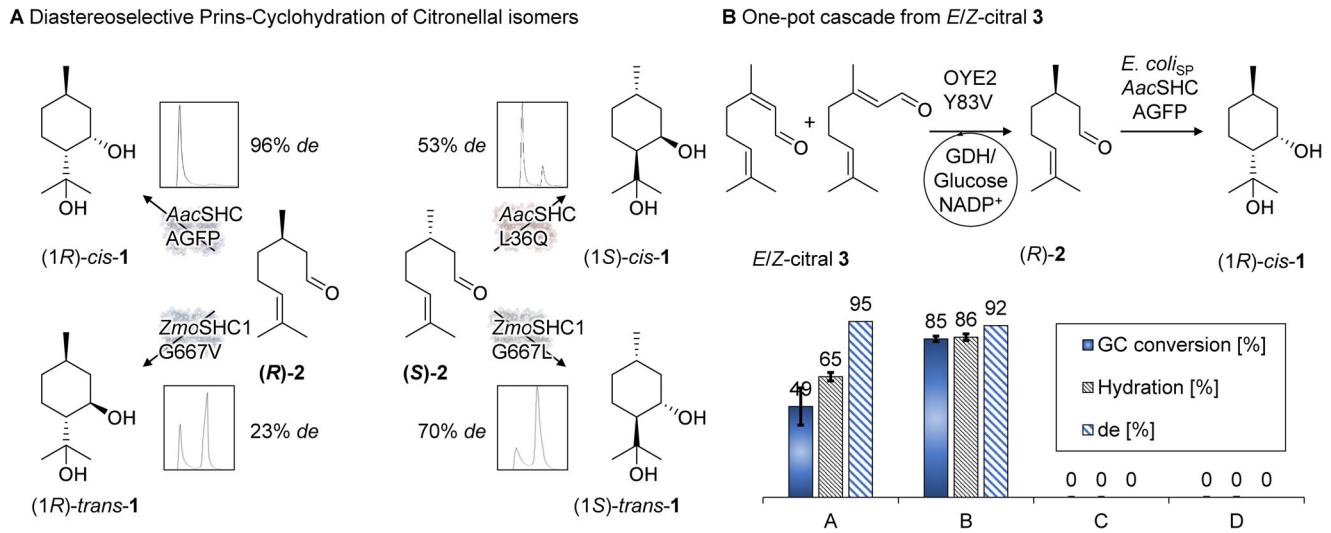


FIGURE 4 | Access to other PMD isomers by SHC homologs and via an ERED/SHC-enzyme cascade. (A) SHC homologs and variants thereof showing the highest diastereoselectivity toward (1*R*)-*cis*-**1** (this work), (1*R*)-*trans*-**1**, (1*S*)-*cis*-**1**, and (1**S**)-*trans*-**1**. The enzymes were produced in earlier projects [37, 38]. Reaction conditions: 1 mM (*R* or *S*)-**2**, 1% DMSO, 50 mg_{CWW}/mL (OD_{600}~ 10) *E. coli* whole cells expressing SHC, 100 mM KF, 10 mM *γ*-cyclodextrin, 40°C, 20 h, 250 rpm. (B) Cascade starting from 60:40 *E/Z*-citral **3** showing (n = 3, blue bars), hydration (n = 3, black striped bars), and diastereomeric access (blue striped bars).Reaction conditions: A: 5 mM *E/Z*-citral **3**, 1% DMSO, 20 mg_{CWW}/mL *E. coli* spheroplasts expressing SHC, 5 μM ERED, 1 mM $NADP^+$, 1 U/mL GDH, 25 mM glucose, 100 mM KF, 10 mM *γ*-cyclodextrin, 40°C, 96 h, 600 rpm (Edmund Bühler Shaker). **B**: same as **A** but 40 mg_{CWW}/mL E. coli spheroplasts expressing SHC. **C**: same as A, but without GDH and glucose. **D**: same as **A**, but without ERED. Please see Figure S5 for ERED solo and Figure S6 for more one-pot experiments. Unless stated otherwise, reported values represent the mean of technical replicates (n as indicated) and error bars denote the standard deviation.

cyclohydration, achieving an unprecedented >96% diastereomeric excess and 91% hydration in the cyclization of (*R*)-citronellal. By systematically engineering squalene-hopene cyclases and combining them with ene-reductases, we unlocked an efficient biocatalytic route to (1*R*)-*cis*-PMD, a stereodefined natural repellent component that serves as a stringent benchmark for analytical and biological evaluation. Beyond this specific transformation, our findings highlight the broader potential of terpene cyclases for taming highly reactive cationic intermediates, which is currently unlocking new frontiers in synthetic chemistry. Future efforts will focus on refining catalyst and cascade robustness, paving the way for a generalizable biocatalytic platform for asymmetric Prins cyclohydration by coupling carbocation control with selective water delivery.

Author Contributions

AS, BH, and CEP designed the project. AS, JR, and PD conducted enzyme engineering. AS and PD did scale-up experiments, mechanistic investigations, and diastereoselective cyclizations. CFC and CEP conducted Ene Reductase experiments. AS, CFC, and CEP conducted cascade experiments. AS drafted the first manuscript.

Acknowledgments

The authors thank BASF for kindly providing (*R*)-citronellal. The authors thank Gen-H for building *E. coli* BL21(DE3) ΔMaeB. The work of BH was funded by the DFG HA 1251/10-1. CFC was funded by the Department of Biotechnology at TU Delft via the Zero-emission Biotechnology (ZEB) Programme.

Conflicts of Interest

Authors AS and BH are co-inventors on patent application EP 23 213 203.5, which is related to this work. The remaining authors declare no competing interests.

Data Availability Statement

The data that support the findings of this study are available from the corresponding author upon reasonable request.

References

1. S. Beermann, G. Dobler, M. Faber, et al., *Journal of Health Monitoring* 8 (2023): 33–61, https://doi.org/10.25646/11401.

2. M. Naddaf, "Mosquito-borne Diseases Are Surging in Europe — How Worried Are Scientists?" *Nature* 633 (2024): 749, https://doi.org/10.1038/d41586-024-03031-y.

3. G. Paluch, L. Bartholomay, and J. Coats, "Mosquito Repellents: A Review of Chemical Structure Diversity and Olfaction," *Pest Management Science* 66 (2010): 925–935, https://doi.org/10.1002/ps.1974.

4. L. Goodyer and S. Schofield, "Mosquito Repellents for the Traveller: Does picaridin Provide Longer Protection Than DEET?" *Journal of Travel Medicine* 25 (2018): S10–S15, https://doi.org/10.1093/jtm/tay005.

5. A. Abd-Ella, M. Stankiewicz, K. Mikulska, et al., "The Repellent DEET Potentiates Carbamate Effects via Insect Muscarinic Receptor Interactions: An Alternative Strategy to Control Insect Vector-borne Diseases," *PLoS ONE* 10 (2015): 1–20, https://doi.org/10.1371/journal.pone.0126406.

6. D. R. Swale, B. Sun, F. Tong, and J. R. Bloomquist, "Neurotoxicity and Mode of Action of N, N-Diethyl-Meta-Toluamide (DEET)," *PLoS ONE* 9 (2014): e103713, https://doi.org/10.1371/journal.pone.0103713.

7. S. S. Garboui, T. G. T. Jaenson, and K. Pålsson, "Repellency of MyggA® Natural Spray (para-menthane-3,8-diol) and RB86 (neem oil) Against the Tick Ixodes Ricinus (Acari: Ixodidae) in the Field in East-central Sweden,"

15213773, 0, Downloaded from https://onlinelibrary.wiley.com/doi/10.1002/anie.88267784 by Tu Delft, Wiley Online Library on [20/04/2026]. See the Terms and Conditions (https://onlinelibrary.wiley.com/terms-and-conditions) on Wiley Online Library for rules of use; OA articles are governed by the applicable Creative Commons License

Experimental and Applied Acarology 40 (2006): 271–277, https://doi.org/10.1007/s10493-006-9031-4.

8. J. F. Anderson, F. J. Ferrandino, M. P. Vasil, R. H. Bedoukian, M. Maher, and K. Mckenzie, "Repellency of Naturally Occurring or Related Compounds, DEET, and Para-Menthane-3,8-Diol to Bed Bugs (Hemiptera: Cimicidae)," *Journal of Medical Entomology* 55 (2018): 666–672, https://doi.org/10.1093/jme/tjx253.

9. S. P. Carroll and J. Loye, "Field Test of a Lemon Eucalyptus Repellent Against Leptoconops Biting Midges," *Journal of the American Mosquito Control Association* 22 (2006): 483–485, https://doi.org/10.2987/8756-971X(2006)22%5b483:FTOALE%5d2.0.CO;2.

10. M. Semmler, F. Abdel-Ghaffar, K. Al-Rasheid, S. Klimpel, and H. Mehlhorn, *Parasitology Research* 106 (2010): 729–731, https://doi.org/10.1007/s00436-009-1698-0.

11. L. G. Borrego, N. Ramarosandratana, E. Jeanneau, et al., "Effect of the Stereoselectivity of Para -Menthane-3,8-diol Isomers on Repulsion Toward Aedes Albopictus," *Journal of Agricultural and Food Chemistry* 69 (2021): 11095–11109, https://doi.org/10.1021/acs.jafc.1c03897.

12. E. Reyes, L. Prieto, U. Uria, L. Carrillo, and J. L. Vicario, "Recent Advances in the Prins Reaction," *ACS Omega* 7 (2022): 31621–31627, https://doi.org/10.1021/acsomega.2c04765.

13. A. Budakoti, P. K. Mondal, P. Verma, and J. Khamrai, "Prins Cyclization-mediated Stereoselective Synthesis of Tetrahydropyrans and Dihydropyrans: An Inspection of Twenty Years," *Beilstein J Org Chem 1777* 17 (2021): 932–963, https://doi.org/10.3762/bjoc.17.77.

14. J. A. A. Grimm, H. Zhou, R. Properzi, et al., *Nature* 615 (2023): 634–639, https://doi.org/10.1038/s41586-023-05747-9.

15. W. M. Hart-Cooper, K. N. Clary, F. D. Toste, R. G. Bergman, and K. N. Raymond, "Selective Monoterpene-Like Cyclization Reactions Achieved by Water Exclusion From Reactive Intermediates in a Supramolecular Catalyst," *Journal of the American Chemical Society* 134 (2012): 17873–17876, https://doi.org/10.1021/ja308254k.

16. I. Zapirain-Gysling, G. Norjmaa, J. D. Maréchal, and G. Ujaque, "Origin of Catalysis by the $[Ga_4\ L_6\ ]^{12-}$ Metallocage on the Prins Reaction," *ACS Catalysis* (2024): 18722–18733, https://doi.org/10.1021/acscatal.4c04696.

17. J. Drapeau, M. Rossano, D. Touraud, et al., "Green Synthesis of Para-Menthane-3,8-diol From Eucalyptus Citriodora: Application for Repellent Products," *Comptes Rendus Chimie* 14 (2011): 629–635, https://doi.org/10.1016/j.crci.2011.02.008.

18. I. Kurnia, A. Yoshida, N. Chaihad, et al., "Synthesis of p -menthane-3,8-diol From Citronellal Over Lignin-derived Carbon Acid Catalysts," *New Journal of Chemistry* 44 (2020): 10441–10447, https://doi.org/10.1039/D0NJ00919A.

19. A. Stanovych, F. Pelissier, C. M. Grison, and C. Grison, "Efficient and Greener Process for the Production of p -Menthane-3,8-diols Using Biosourced Ammonium Salts as Catalysts," *ACS Sustainable Chemistry & Engineering* 11 (2023): 6427–6434, https://doi.org/10.1021/acssuschemeng.3c00334.

20. Y. Yuasa, H. Tsuruta, and Y. Yuasa, "A Practical and Efficient Synthesis of p -Menthane-3,8-diols," *Organic Process Research & Development* 4 (2000): 159–161, https://doi.org/10.1021/op9901036.

21. H. Cheng, X. Meng, R. Liu, et al., "Cyclization of Citronellal to p-menthane-3,8-diols in Water and Carbon Dioxide," *Green Chemistry* 11 (2009): 1227, https://doi.org/10.1039/b823297k.

22. A. Schneider, T. B. Lystbæk, D. Markthaler, N. Hansen, and B. Hauer, "Biocatalytic Stereocontrolled Head-to-tail Cyclizations of Unbiased Terpenes as a Tool in Chemoenzymatic Synthesis," *Nature Communications* 15 (2024): 1–10, https://doi.org/10.1038/s41467-024-48993-9.

23. A. Schneider, J. Ruppert, T. B. Lystbæk, S. Bastian, and B. Hauer, "Expanding the Cation Cage: Squalene-Hopene Cyclase-Mediated Enantioselective Semipinacol Rearrangement," *ACS Catalysis* 13 (2023): 1946–1951, https://doi.org/10.1021/acscatal.2c03835.

24. S. A. Bastian, S. C. Hammer, N. Kreß, B. M. Nestl, and B. Hauer, "Selectivity in the Cyclization of Citronellal Introduced by Squalene Hopene Cyclase Variants," *Chemcatchem* 9 (2017): 4364–4368, https://doi.org/10.1002/cctc.201700734.

25. T. Dwars, E. Paetzold, and G. Oehme, "Reactions in Micellar Systems," *Angewandte Chemie International Edition* 44 (2005): 7174–7199, https://doi.org/10.1002/anie.200501365.

26. A. I. Benítez-Mateos, A. Schneider, E. Hegarty, B. Hauer, and F. Paradisi, "Spheroplasts Preparation Boosts the Catalytic Potential of a Squalene-Hopene Cyclase," *Nature Communications* 13 (2022): 1–9, https://doi.org/10.1038/s41467-022-34030-0.

27. B. Zhang, H. Du, Y. Zheng, et al., "Design and Engineering of Whole-Cell Biocatalyst for Efficient Synthesis of (R)-Citronellal," *Microbial Biotechnology* 15 (2022): 1486–1498, https://doi.org/10.1111/1751-7915.13958.

28. C. Carucci, F. Raccis, A. Salis, and E. Magner, "Specific Ion Effects on the Enzymatic Activity of Alcohol Dehydrogenase From Saccharomyces Cerevisiae," *Physical Chemistry Chemical Physics* 22 (2020): 6749–6754, https://doi.org/10.1039/C9CP06800G.

29. T. Baba, T. Ara, M. Hasegawa, et al., "Construction of Escherichia coli K-12 in-Frame, Single-Gene Knockout Mutants: The Keio Collection," *Molecular Systems Biology* 2 (2006): 2006–2008, https://doi.org/10.1038/msb4100050.

30. H. Land and M. S. Humble, *Methods Molecular Biology* (Humana Press Inc., 2018), 43–67, https://doi.org/10.1007/978-1-4939-7366-8_4.

31. D. Bednar, K. Beerens, E. Sebestova, et al., "FireProt: Energy- and Evolution-Based Computational Design of Thermostable Multiple-Point Mutants," *Plos Computational Biology* 11 (2015): e1004556, https://doi.org/10.1371/journal.pcbi.1004556.

32. M. Musil, J. Stourac, J. Bendl, et al., "FireProt: Web Server for Automated Design of Thermostable Proteins," *Nucleic Acids Research* 45 (2017): W393–W399, https://doi.org/10.1093/nar/gkx285.

33. K. Watanabe and Y. Suzuki, "Protein Thermostabilization by Proline Substitutions," *Journal of Molecular Catalysis B Enzyme* 4 (1998): 167–180, https://doi.org/10.1016/S1381-1177(97)00031-3.

34. T. Zhu, J. Sun, H. Pang, and B. Wu, "Computational Enzyme Redesign Enhances Tolerance to Denaturants for Peptide C-Terminal Amidation," *JACS Au* 4 (2024): 788–797, https://doi.org/10.1021/jacsau.3c00792.

35. P. O. Syrén, S. C. Hammer, B. Claasen, and B. Hauer, "Entropy Is Key to the Formation of Pentacyclic Terpenoids by Enzyme-Catalyzed Polycyclization," *Angewandte Chemie International Edition* 53 (2014): 4845–4849, https://doi.org/10.1002/ange.201402087.

36. A. Schneider, C. Curado, T. B. Lystbaek, S. Osuna, and B. Hauer, "Harnessing the Structure and Dynamics of the Squalene-Hopene Cyclase for (−)-Ambroxide Production**," *Angewandte Chemie International Edition* 62 (2023): e202301607, https://doi.org/10.1002/anie.202301607.

37. S. Henche, B. M. Nestl, and B. Hauer, "Enzymatic Friedel-Crafts Alkylation Using Squalene-Hopene Cyclases," *Chemcatchem* 13 (2021): 3405–3409, https://doi.org/10.1002/cctc.202100452.

38. S. C. Hammer, A. Marjanovic, J. M. Dominicus, B. M. Nestl, and B. Hauer, "Squalene Hopene Cyclases Are Protonases for Stereoselective Brønsted Acid Catalysis," *Nature Chemical Biology* 11 (2015): 121–126, https://doi.org/10.1038/nchembio.1719.

39. C. Ferrer-Carbonell, R. Villa, I. Viskaal, D. J. Opperman, and C. E. Paul, "Enzymatic Synthesis of Enantiopure (R)-Citronellal From Geraniol via a Short-Chain Dehydrogenase and Ene Reductase," *Advanced Synthesis & Catalysis* 367 (2025): e202500060, https://doi.org/10.1002/adsc.202500060.

15213773, 0, Downloaded from https://onlinelibrary.wiley.com/doi/10.1002/anie.8825784 by Tu Delft, Wiley Online Library on [20/04/2026]. See the Terms and Conditions (https://onlinelibrary.wiley.com/terms-and-conditions) on Wiley Online Library for rules of use; OA articles are governed by the applicable Creative Commons License

40. "BASF to Invest in Its Aroma Ingredients Business by Expanding Its Global Production Footprint With New Plants in China and Germany," can be found under https://www.basf.com/global/en/media/news-releases/2023/03/p-23-129.

Supporting Information

Additional supporting information can be found online in the Supporting Information section.

Supporting File: anie71986-sup-0001-SuppMat.docx.

15213773, 0, Downloaded from https://onlinelibrary.wiley.com/doi/10.1002/anie.88267B4 by Tu Delft, Wiley Online Library on [20/04/2026]. See the Terms and Conditions (https://onlinelibrary.wiley.com/terms-and-conditions) on Wiley Online Library for rules of use; OA articles are governed by the applicable Creative Commons License